Hindawi
Complexity
Volume 2019, Article ID 7672930, 10 pages
https://doi.org/10.1155/2019/7672930

Research Article

Buoyancy Force Acting on Underground Structures considering Seepage of Confined Water

Ji-wen Zhang,[1,2] Jie Cao,[2,3] Linlong Mu,[4,5] Le Wang,[4,5] and Jie Li[4,5]

[1]*School of Human Settlements and Civil Engineering, Xi'an Jiaotong University, Xi'an, Shanxi 710049, China*
[2]*China JIKAN Research Institute of Engineering Investigations and Design, Co, Ltd, Xi'an, Shanxi 710043, China*
[3]*Shaanxi Key Laboratory of Engineering Behaviour and Foundation Treatment for Special Soil, Xi'an, Shaanxi 710043, China*
[4]*Key Laboratory of Geotechnical and Underground Engineering of the Ministry of Education, Tongji University, Shanghai 200092, China*
[5]*Department of Geotechnical Engineering, Tongji University, Shanghai 200092, China*

Correspondence should be addressed to Linlong Mu; mulinlong@tongji.edu.cn

Received 25 September 2018; Revised 12 December 2018; Accepted 1 January 2019; Published 13 January 2019

Academic Editor: Dimitri Volchenkov

The antifloating property of underground structures in areas with high underground water levels is a key design aspect. Evaluating the buoyancy forces acting on underground structures is complicated, particularly in the presence of confined water beneath the structures. Herein, the effects of the permeability coefficient of layered soil, hydraulic gradient, and embedment depth of the aquiclude on the buoyancy force acting on underground structures are investigated through three model tests: (1) calibration of the test system, (2) buoyancy force acting on a structure located in homogeneous soil considering vertical direction seepage, and (3) buoyancy force acting on a structure located in layered soil considering vertical seepage of confined water. The results show that the pore pressure along the structure and the buoyancy force acting on the underground structure considering seepage are greater than those obtained under hydrostatic conditions. The raising ratios of the pore pressure and buoyancy force are equal to the vertical hydraulic gradient when seepage occurs in homogeneous soil. In the presence of confined water, the raising ratio is significantly greater than the hydraulic gradient. In the cases studied herein, the raising ratio is approximately twice the hydraulic gradient. Simplified equations are proposed to calculate the buoyancy force acting on underground structures considering the vertical seepage of confined water. Finally, a finite element analysis is carried out to verify the conclusions obtained from the model test and the rationality of the proposed equations.

1. Introduction

The antifloating design of underground structures is an important aspect in underground engineering. Large underground structures, such as underground garage of high-rise buildings and underground pipe galleries, in high-level underground water level are exposed to high buoyancy forces, which may uplift underground structures [1–3], particularly those located in confined water. The reasonable estimation of the buoyancy forces acting on underground structures in complex geological and hydrological conditions is important to the safety of such structures.

The buoyancy force without considering the effect of seepage can be calculated in two steps: (1) reasonably determining the underground water level and (2) calculating the buoyancy force based on Archimedes' principle. However, many researches showed that the measured buoyancy forces acting on underground structures are lower than those obtained based on the Archimedes' principle [4–7]. The buoyancy force acting on an underground structure depends on many factors; e.g., the liquefaction of sand during an earthquake usually leads to a sudden increase in the buoyancy force [8–10]. For cohesive soils, the buoyancy force would reduce because of the interaction of the soil particles and water at a microscopic level [7, 11, 12]. Seepage flow is found to influence the buoyancy force acting on underground structures [13]. The pore water pressure in soil, which changes the magnitude of the buoyancy force acting

Table 1: Engineering properties of the foundation soil.

Engineering properties	Symbol	Unit	Fine sand	Clay
Wet density	ρ	$kg{\cdot}m^{-3}$	1960	2010
Dry density	ρ_d	$kg{\cdot}m^{-3}$	1630	1710
Void ratio	e	-	0.64	0.65
Plasticity index	Ip	-	/	8.8
Liquid index	I_l	-	/	0.38
Permeability coefficient	k	$m{\cdot}s^{-1}$	5.35×10^{-5}	7.11×10^{-7}

on underground structures, is significantly influenced by the seepage flow. Many studies have investigated seepage flow and the corresponding pore pressure induced by seepage [14–16]. Seepage leads to a change in the force acting on underground structures because of the change in the pore pressure. The complex foundation–soil–water interaction behaviour is not fully understood [17–24]. Studies on the effect of seepage on the buoyancy force acting on underground structures are limited.

In some urban areas of China, such as Beijing, Shanghai, and Wuhan, the underground hydrological conditions are complex. Multilayer confined water with a high confined water head is observed [25]. The seepage of confined water changes the pore pressure distribution and the buoyancy force acting on the structures. Studies have investigated the seepage of confined water in layered soil [26–28]. The force acting on structures induced by seepage in a homogeneous soil is usually horizontal, whereas the force acting on structures induced by the seepage of confined water in layered soil is vertical. The floating potential of underground structures induced by vertical seepage of confined water is significantly greater than that induced by normal seepage in one soil layer. The influence of confined-water seepage on the buoyancy force acting on underground structures is more complicated than that of the horizontal seepage. Unfortunately, no study has been carried out to understand the influence of vertical seepage of confined water on the buoyancy force acting on underground structures. To estimate the buoyancy force acting on underground structures located in layered soil with confined water, we need to first study the influence of seepage of confined water on the buoyancy force acting on such structures.

In this paper, we study the influence of vertical seepage of confined water on the buoyancy force acting on underground structures in different soil configurations and hydraulic gradients through model tests. The relationship between the pore pressure, buoyancy force, and hydraulic gradient under vertical seepage in homogeneous sand and layered soils is investigated. Simplified equations are proposed to calculate the buoyancy force acting on the underground structures considering the effect of vertical seepage. Further, a series of FEM studies are carried out to validate the experimental findings and the rationality of the equations.

2. Experimental Setup and Procedure

2.1. Experimental Setup. Figure 1 shows the experimental apparatus used in this study. The apparatus comprises four main parts: a tank, a water supply circulation system, a model of the underground structure, and a measuring system. The inner size of the tank is 600 mm × 600 mm × 1000 mm (width × length × depth), as shown in Figure 2. The water supply circulation system includes a vertical steel frame with a height of 1.5 m, two suspended water tanks, which control the water levels at the upper and lower bored pipes in the tank, a sink for overflows during the test, and a submersible pump that pumps the water to the upper water tank. The upper bored pipe is 120 mm from the top of the tank, and the lower bored pipe is 80 mm from the bottom of the tank. The difference in the water levels between the upper and lower bored pipes can cause a steady vertical seepage field in the soil.

Figure 3 shows the model of the underground structure with dimensions of 200 mm × 200 mm × 400 mm (width × length × depth). It is made of 10 mm thick plastic plates. To accurately measure the buoyancy force acting on the bottom of the model, the base of the model is separated from the sides of the model. The base is connected to the sides of the model using waterproof rubber and can move freely in the vertical direction when subjected to buoyancy forces. Therefore, the soil–structure friction can be neglected when measuring the buoyancy force acting on the bottom of the structure during the test. The buoyancy measuring system comprises a reaction frame fixed to the tank, a force-measuring ring with a range of 0.6 kN, a dial indicator, and a force-transmitting rod with four legs, which transfer the force acting on the base of the structure to the force-measuring ring. Six micro-pore-pressure sensors are located around the model structure, as shown in Figure 4. The measuring range and the accuracy of the sensors are 20 and 0.04 kPa, respectively. Sensor 'A' is used to measure the pore pressure at the centre of the model underneath the base, and sensors 'B', 'C', 'D', 'E', and 'F' are used to measure the pore pressure around the corners of the structure at depths of 200, 300, 400, 500, and 600 mm, respectively. The data are recorded using the DataTaker DT85.

Fine sand and clay obtained from Shanghai were used to form the foundation in the test. Table 1 lists the wet density, dry density, void ratios, plasticity index, liquid index, and permeability coefficient of the soil compacted in the tank. The ratio of the permeability coefficient of fine sand to that of clay is 75.25. Therefore, fine sand is used to form the aquifer, and clay is used to form the overlying aquiclude.

2.2. Procedure. Seven tests, divided into three series, were carried out, as listed in Table 2. The embedment depth of the structure in the soil is 300 mm.

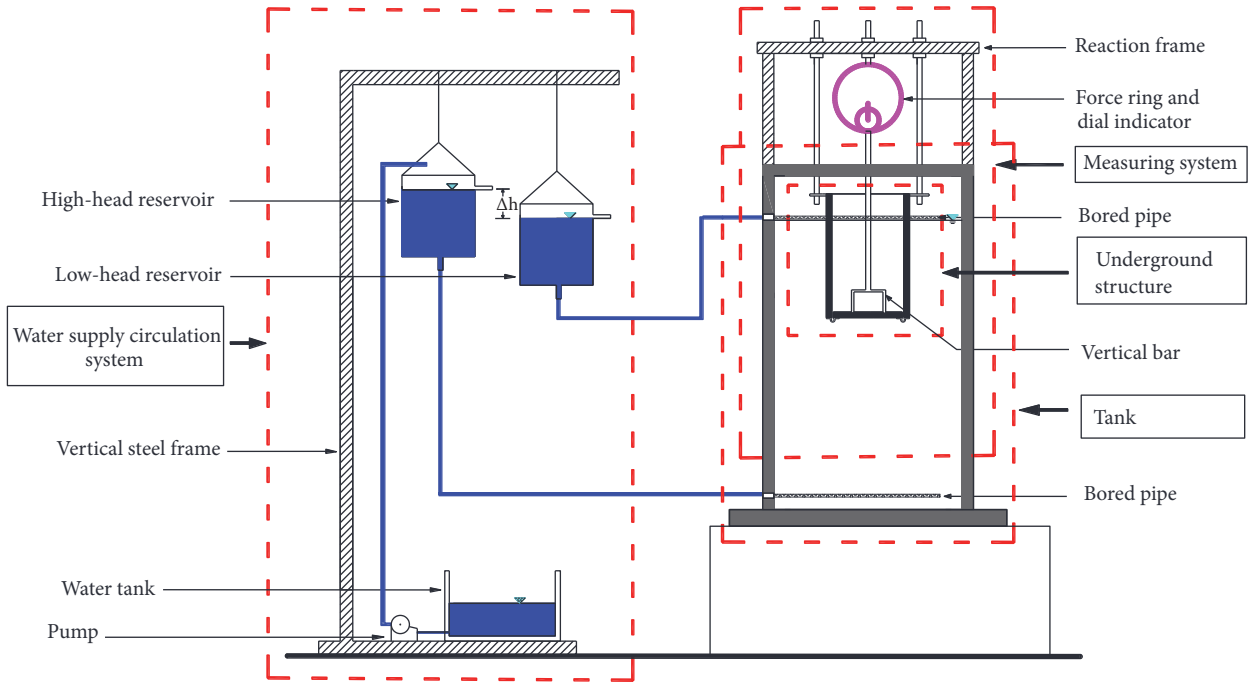

Figure 1: Experimental setup.

Figure 2: Image of the tank.

Table 2: Summary of system calibration, homogeneous soil layer, and overlying aquiclude tests.

Test series	Test case	Description
System calibration	S0	The structure is placed in pure water.
Homogeneous sand	H1	The structure is embedded in fine sand, and the water head difference is 0.
	H2	The structure is embedded in fine sand, and the water head difference is 10 cm.
	H3	The structure is embedded in fine sand, and the water head difference is 20 cm.
Layered soil with confined water	O4	The structure is embedded in overlying aquiclude, and the water head difference is 0.
	O5	The structure is embedded in overlying aquiclude, and the water head difference is 10 cm.
	O6	The structure is embedded in overlying aquiclude, and the water head difference is 20 cm.

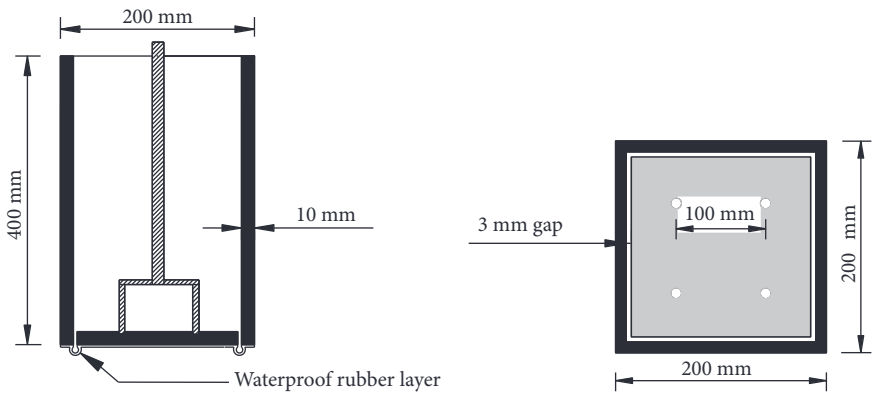

(a) Section plan of the model (b) Plan of the model

Figure 3: Model of the underground structure.

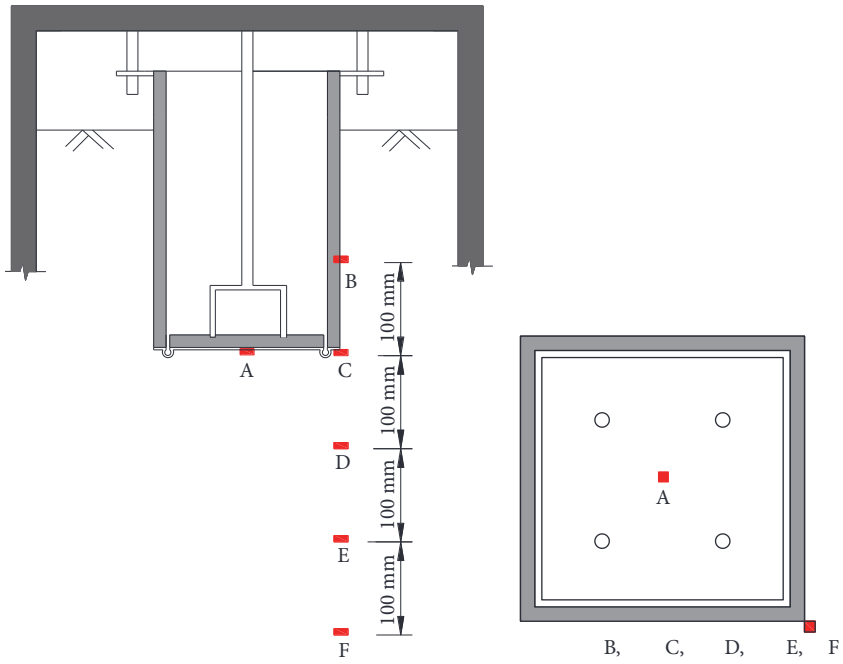

(a) Section plan (b) Plan

Figure 4: Layout of the pore pressure sensor.

The case S0 corresponds to 'system calibration.' In this case, the underground structure model was placed in pure water. Four steps were carried out in this test. In the first step, the structure was slowly immersed in water until the embedment depth reached 300 mm. In the second step, the water level was lowered to the bottom of the structure. In the third step, the water level was raised until the embedment depth of the structure reached 300 mm. In the fourth step, the water level was lowered to the bottom of the structure again. The water level was adjusted by adjusting the height of the water tanks.

The cases H1–H3 correspond to 'homogeneous sand' and were considered to investigate the effects of the hydraulic gradient on the pore pressure and buoyancy force acting on the underground structure placed on homogeneous fine sand. The total depth of the sand is 900 mm. The embedment depth of the structure is 300 mm. The water head height of the lower bored pipe is higher than that of the upper bored pipe. The corresponding hydraulic gradients are 0, 0.125, and 0.25, respectively.

The cases O4–O6 correspond to 'layered soil with confined water' and were considered to investigate the influence of the overlying aquiclude on the buoyancy force acting on the structure. Here, the total depth of the soil is 900 mm. A 400 mm thick clay layer was placed over a 500 mm thick sand layer. The embedment depth of the structure is 300 mm. The corresponding hydraulic gradients for cases O4–O6 are 0, 0.125, and 0.25, respectively.

Table 3: Measured and theoretical pore pressures and buoyancy forces acting on the structure placed on homogeneous soil layer.

Test case	Hydraulic gradient	Measured pore pressure from 'a,' P_c (kPa)	Theoretical hydrostatic pore pressure, P_0 (kPa)	Pore pressure raising ratio, P_c/P_0-1	Measured buoyancy force, F (N)	Theoretical hydrostatic buoyancy force, F_0 (N)	Buoyancy force raising ratio, F/F_0-1
H1	0	3.105	3.0	0.035	128	120	0.067
H2	0.125	3.509	3.0	0.170	144	120	0.200
H3	0.25	4.101	3.0	0.367	164	120	0.367

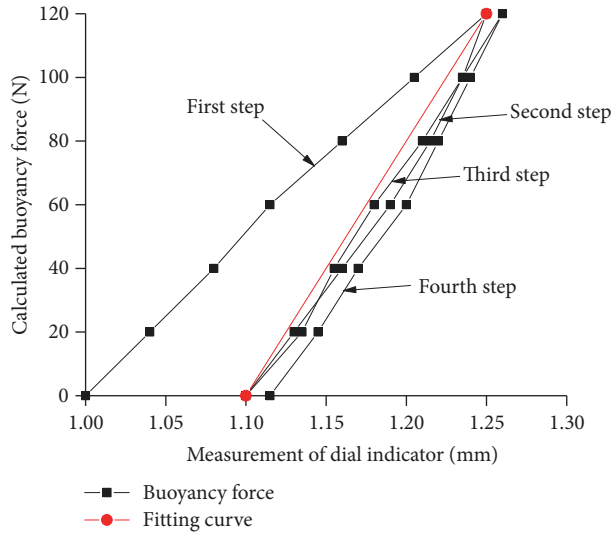

Figure 5: Calibration result of the buoyancy force.

3. Test Results

3.1. System Calibration. The pore pressure and buoyancy force acting on the model bucket can be calculated from Archimedes' principle using (1) and (2), respectively. Figure 5 shows the relationship between the calculated buoyancy force and the measured deformation of the base of the structure.

The relationships between the buoyancy force and the measured deformation obtained from steps 2–4 are the same, whereas that obtained from step 1 is different. This may be because the system filled the initial gap between the various components of the mechanism in the first step. The system becomes more accurate and stable, making the test repeatable. The buoyancy force acting on the structure can be calculated from the measured deformation of the base using (3).

$$P_0 = \rho g h \quad (1)$$

$$F_0 = P_0 A \quad (2)$$

$$F = 800s - 880 \quad (3)$$

where ρ is the density of water, g is the acceleration due to gravity, h is the hydrostatic water head, A is the cross-sectional area of the model bucket, and s is the deformation measured using the dial indicator.

3.2. Structure in Homogeneous Soil. Figure 6 shows the pore pressure around the corners of the structure at different depths in terms of the measured pore pressure (P) and the raising ratio of pore pressure (P/P_0-1). P_0 is the theoretical pore pressure calculated using (1). The measured pore pressure of test H1 is consistent with the theoretical hydrostatic pressure. The measured pore pressures from H2 and H3 are significantly greater than the theoretical hydrostatic pressure. The pore pressure is significantly influenced by the vertical seepage of the underground water. The pore pressure distribution along the depth remains linear. The raising ratio of the pore pressure along the depth is approximately constant, and the fluctuated amplitude is within 0.05, probably because of sensor fluctuation. The raising ratios of the pore pressure in tests H2 and H3 are approximately 0.14 and 0.29, respectively. The raising ratio is approximately equal to the vertical hydraulic gradient. The buoyancy force acting on the structure under seepage should be calculated from the highest water head in the hydraulically connected area and not from the water head height around the structure.

Table 3 presents the pore pressure at the centre of the base slab under the structure (P_c) and the buoyancy force acting on the base slab (F). The pore pressure raising ratio (P_c/P_0-1) at the centre of the slab is slightly greater than the hydraulic gradient. Compared with the pore pressure measured using sensor 'b', as shown in Figure 6(a), the pore pressure raising ratio at the centre of the structure is generally

Table 4: Measured and theoretical pore pressures and buoyancy forces acting on the structure placed on overlying aquiclude.

Test case	Hydraulic gradient	Measured pore pressure from 'a', P_c (kPa)	Theoretical hydrostatic pore pressure, P_0 (kPa)	Pore pressure raising ratio, P_c/P_0-1	Measured buoyancy force, F (N)	Theoretical hydrostatic buoyancy force, F_0 (N)	Buoyancy force raising ratio, F/F_0-1
O4	0	2.945	3.0	−0.018	128	120	0.067
O5	0.125	3.724	3.0	0.241	152	120	0.267
O6	0.25	4.640	3.0	0.547	180	120	0.500

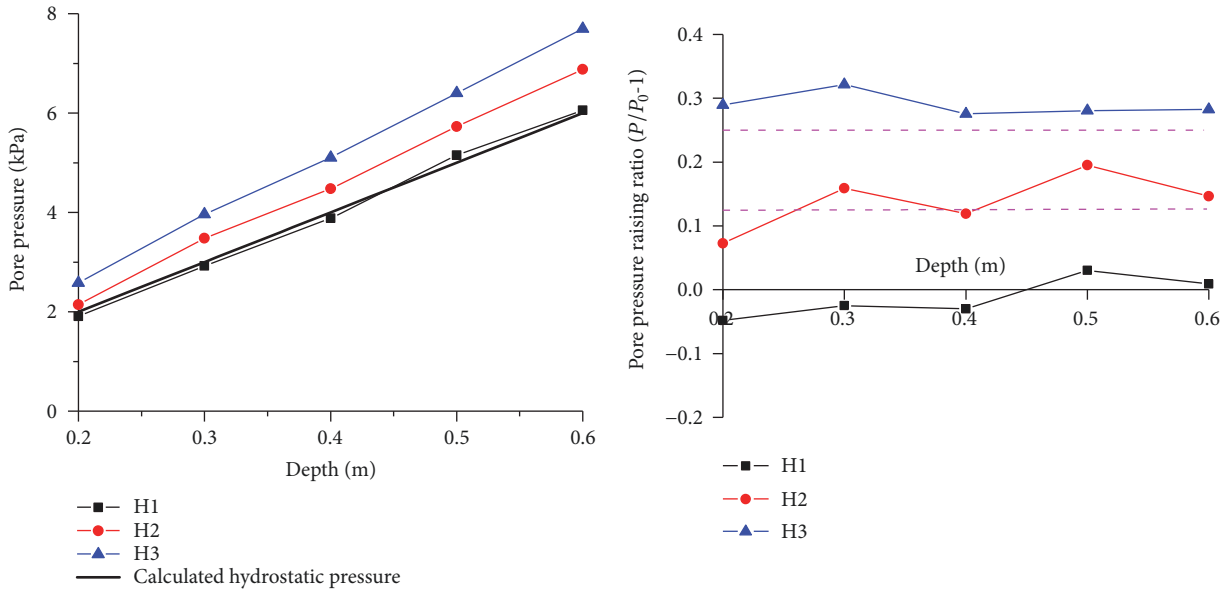

(a) Measured pore pressure values

(b) Raising ratios of the pore pressure

Figure 6: Measured pore pressure at different depths in structural corner position.

greater than that around the corner of the structure under the same condition. Similarly, the raising ratio of the buoyancy force (F/F_0-1) is greater than the hydraulic gradient. The raising ratio of the buoyancy force is consistent with the raising ratio of the pore pressure at the centre of the structure. Nevertheless, we believe it is acceptable from an engineering standpoint to use the hydraulic gradient to calculate the buoyancy force, as shown in (4).

$$F_0 = (1 + i)\,\rho g h A \tag{4}$$

where i is the hydraulic gradient.

3.3. Structure in Overlying Aquiclude. Figure 7 shows the pore pressure in the 'layered soil with confined water' test, in which the underground structure is placed on the overlying aquiclude. The same conclusion can be drawn from hydrostatic test O1; i.e., the measured pore pressure is consistent with the theoretical hydrostatic pressure in the absence of seepage. The measured pore pressures are significantly greater than the theoretical hydrostatic pressure in the presence of a vertical seepage field in the tests. Unlike the results obtained when considering a homogeneous soil layer, the pore pressure curves along the depth in tests O2 and O3 become fold lines. The slope of the curve for the overlying aquiclude is greater than that for the deeper sand layer. In other words, the pore pressure in aquiclude reduces with depth much more quickly than that in sand. For tests O2 and O3, the raising ratio of the pore pressure is largely consistent when the depth is less than 0.4 m; this is similar to the results obtained under homogeneous sand. However, the raising ratio of the pore pressure decreases with the increase in the depth when the depth is greater than 0.4 m, which is located in the sand layer. The pore pressures induced by seepage in homogeneous sand and in layered soil with confined water are different. The maximum raising ratios of the pore pressure at the soil interface are 0.23 and 0.52 for O2 and O3, respectively. The maximum raising ratio of the pore pressure is approximately twice the hydraulic gradient. The pore pressure distribution along the depth is no longer linear as expected, making it unsafe to calculate the buoyancy force acting on the structure from the hydrostatic water level based on the current design method.

Table 4 lists the pore pressure at the centre of the structure and the buoyancy force acting on the base of the structure (F). The raising ratio of the pore pressure is approximately twice the hydraulic gradient and is slightly greater than the raising ratio of the pore pressure around the corners of

Table 5: Material parameters used in FEM simulation.

Engineering properties	Symbol	Unit	Fine sand	Clay
Saturated gravity	γ	kN/m^3	19.6	20.1
Young's modulus	E	MPa	25	40
Void ratio	ν		0.3	0.25
Permeability coefficient	k	m·s^{-1}	5.35×10^{-5}	7.11×10^{-7}

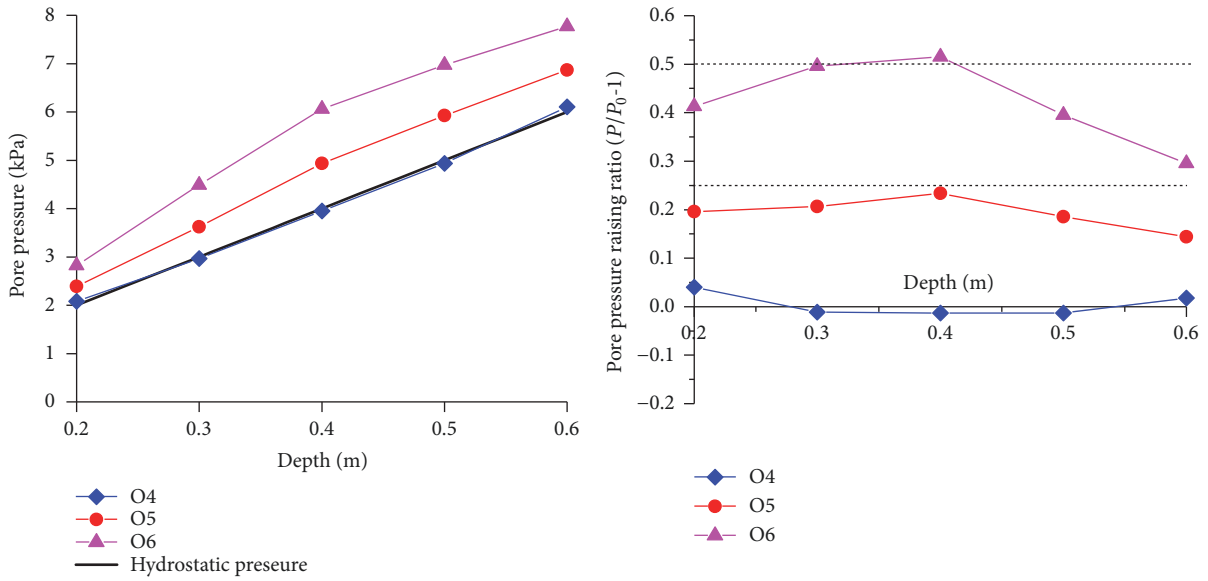

(a) Measured pore pressure

(b) Raising ratio of the pore pressure

Figure 7: Pore pressure at different depths.

the structure at the same depth (300 mm), as shown in Figure 7(b). The raising ratio of the buoyancy force acting on the base is similar to that of the pore pressure at the centre of the structure. The buoyancy force acting on the structure is significantly increased because of the effect of the overlying aquiclude or confined water. Compared with the structure placed on homogeneous sand, the increment in the buoyancy force acting on the structure is twice as that obtained from hydraulic gradient calculation when the structure is subjected to overflowing confined water. The buoyancy acting on the structure can be calculated using (5).

$$F_0 = (1 + 2i)\,\rho g h A \tag{5}$$

4. Numerical Simulation

4.1. Finite Element Model. ABAQUS/Standard was used to carry out a 3D simulation of the tests. The seepage calculation module of ABAQUS was employed. The soil was set as porous material. Table 5 lists the parameters of the soil. Figure 8 shows the meshed model. The soil element was set as the pore pressure element, i.e., C3D8P. The dimension of the mesh is the same as that of the model test. The side and bottom boundaries were set as impermeable boundaries. The top boundary was set as a free boundary. The interfaces between the structure and the soil were set as impermeable boundaries. This ensures that the water will not flow into the structure. The water head heights at the bottom and top were set according to the test cases H1, H2, and H3 and O1, O2, and O3. The buoyancy force was calculated by integrating the pore pressures at the lower surface of the base. The other conditions were the same as those in the model tests.

4.2. Results of FEM. Figure 9 presents the pore pressure around the corners of the structure at different depths. Figure 10 shows the pore pressure at the centre of the structure under the base. The results of the model tests and FEM are in good agreement. The effect of the overlying aquiclude on the pore pressure in an overflow field of confined water obtained from FEM is the same as that obtained from the model tests.

The buoyancy forces obtained from the model tests, FEM, and proposed equations, as shown in Figure 11, are in good agreement. Therefore, it is feasible to use the steady-state seepage module of the ABAQUS/standard to calculate the pore pressure and buoyancy force. Equations (3) and (4) are simplified solutions to calculate the buoyancy force acting on structures located in a confined water stratum subjected to seepage.

5. Conclusions

In this study, the buoyancy force and pore pressure acting on an underground structure considering vertical seepage

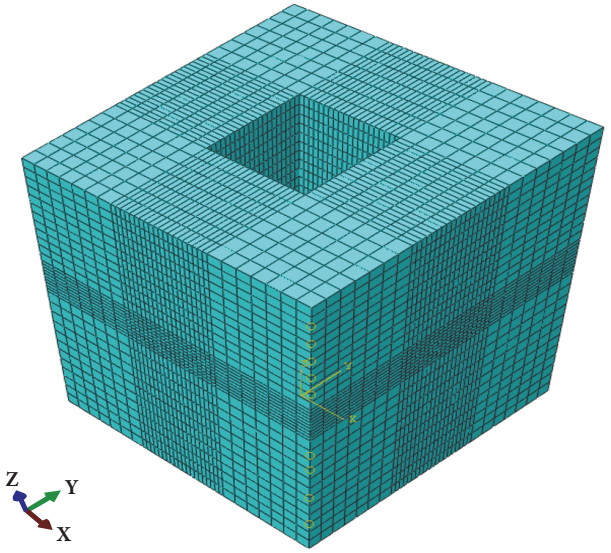

Figure 8: Schematic of the finite element mesh.

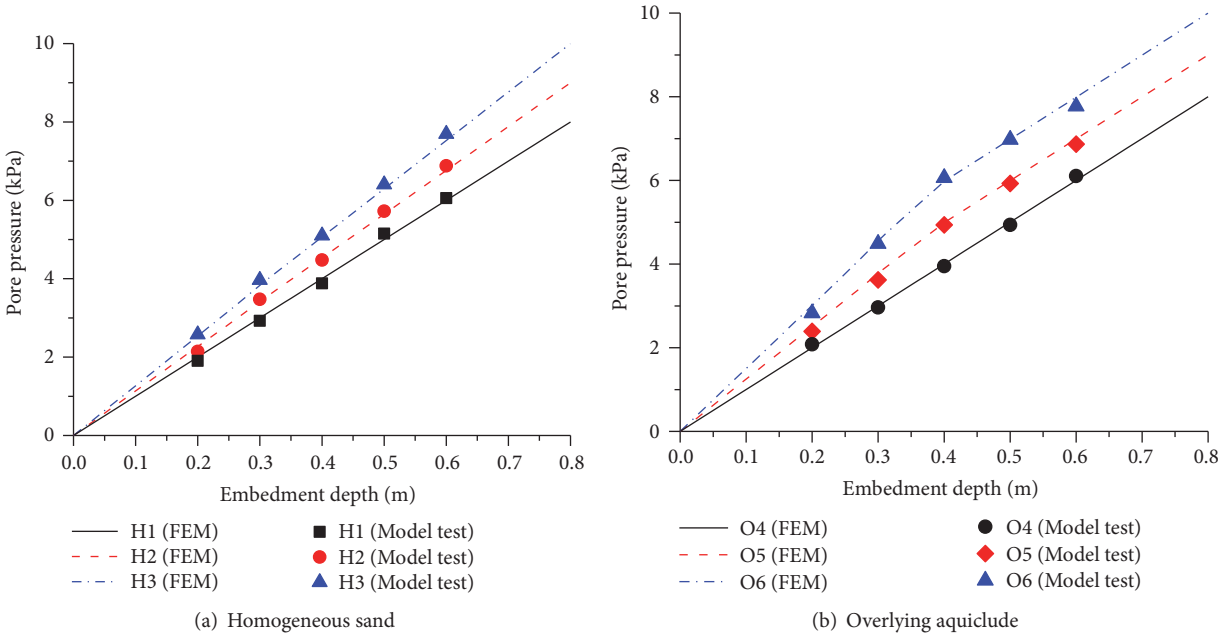

Figure 9: Comparison between measured pore pressure values and finite element results at corner positions.

were investigated by conducting model tests and numerical simulation. The test results demonstrated that the pore pressure around the underground structure and the buoyancy force acting on it considering the vertical seepage (of the overflowing confined water through the overlying aquiclude) are significantly greater than those obtained under the hydrostatic condition. For the structure placed on a homogeneous permeable soil layer, the raising ratios of the buoyancy force and pore pressure were approximately equal to the vertical hydraulic gradient. The buoyancy force acting on the structure placed on an overlying aquiclude was greater than that acting on the structure placed on homogeneous sand. The pore pressure raising ratio was maximum at the interface of the two soil layers and was approximately twice the hydraulic gradient. Two equations were proposed to calculate the buoyancy force acting on the underground structures considering the seepage of overflowing confined water. The results of the model tests and the rationality of the equations were verified by conducting FEM simulation. The equations were found to be feasible to calculate the buoyancy force acting on underground structures considering the vertical seepage of overflowing confined water. Unfortunately, the seepage is not always vertical in practice, and the leakage of the confined water which may cause the reduction on friction

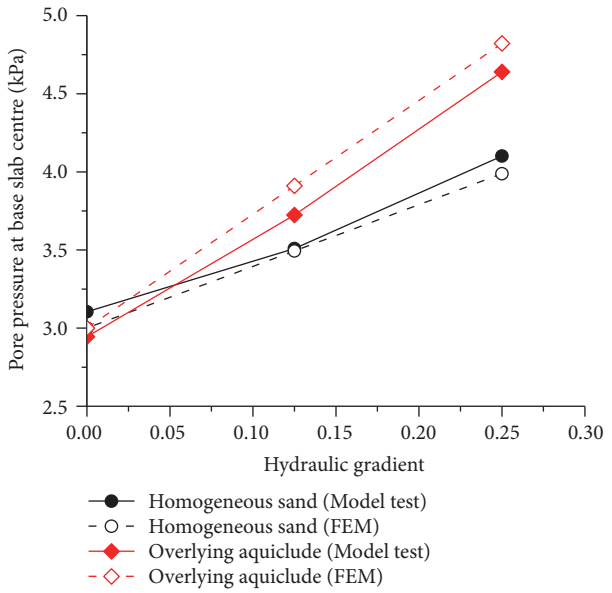

Figure 10: Comparison between measured pore pressure values and finite element results at base slab centre.

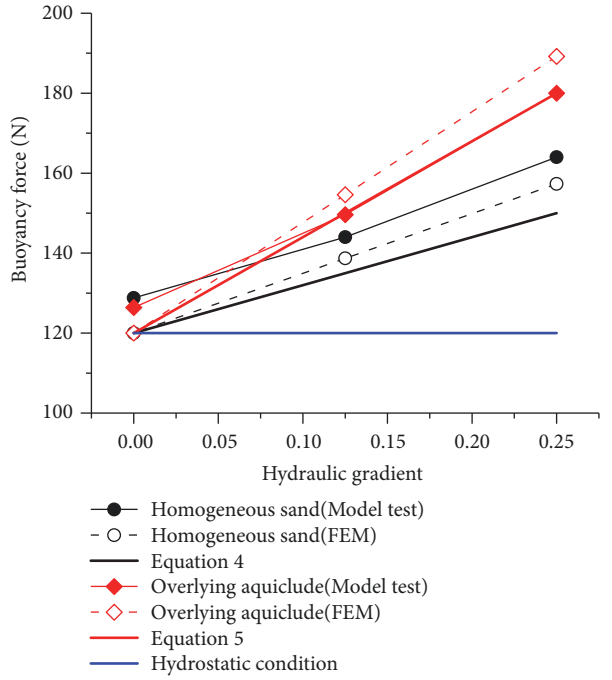

Figure 11: Comparison between measured buoyancy force values and finite element results.

stress along the underground structure is not considered. The proposed equations are not enough for antifloating design although they are helpful to calculate the buoyancy force acting on the base of the underground structure considering the vertical seepage.

Data Availability

The data in the manuscript is obtained directly from the tests and the FEM software. So the data in the manuscript is direct data and is reliable.

Conflicts of Interest

The authors declare that they have no conflicts of interest.

Acknowledgments

The research is under the support of Shaanxi Science and Technology Coordination Innovation Project Plan (2016KTZDSF03-02) and the Fundamental Research Funds for the Central Universities.

References

[1] J. Li and W. Sun, "Study on design of uplift piles and calculation of float in underground structures," *Structural Engineering International*, vol. 23, no. 2, pp. 80–84, 2007.

[2] I. H. Wong, "Methods of resisting hydrostatic uplift in substructures," *Tunnelling and Underground Space Technology*, vol. 16, no. 2, pp. 77–86, 2001.

[3] H. E. Acosta-Martinez, S. Gourvenec, and M. F. Randolph, "Centrifuge study of capacity of a skirted foundation under eccentric transient and sustained uplift," *Géotechnique*, vol. 62, no. 4, pp. 317–328, 2012.

[4] Y. Cui, J. H. Cui, and S. H. Wu, "Model test of underground structure buoyant," *Spec. Struct*, vol. 16, no. 1, pp. 32–36, 1999.

[5] P. F. Zhou, *Groundwater uplift mechanism study under complex urban environment [MS thesis]*, China University of Geosciences, Beijing, China, 2006.

[6] Y. S. Fang, "Discussion on pore pressure and related problems considering hydraulic pressure ratio," *Geotech. Eng. World*, vol. 10, no. 5, pp. 21–26, 2007.

[7] L. Song, X. Kang, and G. Mei, "Buoyancy force on shallow foundations in clayey soil: An experimental investigation based on the "Half Interval Search"," *Ocean Engineering*, vol. 129, pp. 637–641, 2017.

[8] H. B. Seed, I. M. Idriss, and I. Arango, "Evaluation of liquefaction potential using field performance data," *Journal of Geotechnical Engineering*, vol. 109, no. 3, pp. 458–482, 1983.

[9] Y. Mohri, N. Fujita, and T. Kawabata, "A simulation on uplift resistance of buried pipe by DEM," in *Proceedings of the Pipelines 2001: Advances in Pipeline Engineering and Construction*, pp. 1–12, California, Calif, USA, July 2001.

[10] S. Suenaga, Y. Mohri, and K. Matsushima, "Performance of Shallow Cover Method with Geogrid at Large Blasting Test," in *Proceedings of the Pipeline Engineering and Construction International Conference 2003*, pp. 648–657, Baltimore, Maryland, United States, 2003.

[11] G. Achari, R. C. Joshi, L. R. Bentley, and S. Chatterji, "Prediction of the hydraulic conductivity of clays using the electric double layer theory," *Canadian Geotechnical Journal*, vol. 36, no. 5, pp. 783–792, 1999.

[12] P. N. Singh and W. W. Wallender, "Effects of adsorbed water layer in predicting saturated hydraulic conductivity for clays with Kozeny-Carman equation," *Journal of Geotechnical and Geoenvironmental Engineering*, vol. 134, no. 6, pp. 829–836, 2008.

[13] Z. Zhang, B. Sun, and H. Xu, "Effect of characteristics of ground water distribution and seepage on anti-uplift analysis of building foundations," *China Civil Engineering Journal*, vol. 34, no. 1, pp. 73–78, 2001.

[14] O. C. Zienkiewicz, P. Mayer, and Y. K. Cheung, "Solution of anisotropic seepage by finite elements," *Journal of the Engineering Mechanical Division*, vol. 92, no. 1, pp. 111–120, 1966.

[15] S. P. Neuman, "Saturated-unsaturated seepage by finite elements," *Journal of the Hydraulics Division*, vol. 99, no. 12, pp. 2233–2250, 1973.

[16] J. D. Rice and J. M. Duncan, "Findings of case histories on the long-term performance of seepage barriers in dams," *Journal of Geotechnical and Geoenvironmental Engineering*, vol. 136, no. 1, pp. 2–15, 2010.

[17] M. E. Harr, *Groundwater and Seepage*, McGraw-Hill, New York, NY, USA, 1962.

[18] D. S. Jeng, L. Li, and D. A. Barry, "Wave-induced seepage flux into anisotropic seabeds," *International Journal for Numerical and Analytical Methods in Geomechanics*, vol. 25, no. 8, pp. 771–787, 2001.

[19] P. Hazelton and B. Murphy, *Interpreting Soil Test Results*, CSIRO, Collingwood, 2007.

[20] J.-J. Wang, H.-P. Zhang, H.-J. Chai, and J.-G. Zhu, "Seismic passive resistance with vertical seepage and surcharge," *Soil Dynamics and Earthquake Engineering*, vol. 28, no. 9, pp. 728–737, 2008.

[21] S. Siddiqua, J. A. Blatz, and N. C. Privat, "Evaluating the behaviour of instrumented prototype rockfill dams," *Canadian Geotechnical Journal*, vol. 50, no. 3, pp. 298–310, 2013.

[22] M. Veiskarami and A. Zanj, "Stability of sheet-pile walls subjected to seepage flow by slip lines and finite elements," *Géotechnique*, vol. 64, no. 10, pp. 759–775, 2014.

[23] P. J. Santos and P. L. A. Barros, "Active earth pressure due to soil mass partially subjected to water seepage," *Canadian Geotechnical Journal*, vol. 52, no. 11, pp. 1886–1891, 2015.

[24] Z. Hu, Z. Yang, and S. Wilkinson, "Analysis of passive earth pressure modification due to seepage flow effects," *Canadian Geotechnical Journal*, vol. 55, no. 5, pp. 666–679, 2018.

[25] P. Zhou, *Groundwater uplift mechanism under complex urban environment [Ph.D. thesis]*, China Geologic University, Beijing, China, 2006.

[26] O. D. L. Strack and H. M. Haitjema, "Modeling double aquifer flow using a comprehensive potential and distributed singularities: 2. Solution for inhomogeneous permeabilities," *Water Resources Research*, vol. 17, no. 5, pp. 1551–1560, 1981.

[27] Y.-S. Xu, S.-L. Shen, Y.-J. Du, J.-C. Chai, and S. Horpibulsuk, "Modelling the cutoff behavior of underground structure in multi-aquifer-aquitard groundwater system," *Natural Hazards*, vol. 66, no. 2, pp. 731–748, 2013.

[28] B. Karchewski, A. Pekinasova, D. Stolle, and P. Guo, "Investigation of a hybrid polygonal finite element formulation for confined and unconfined seepage," *International Journal for Numerical and Analytical Methods in Geomechanics*, vol. 40, no. 12, pp. 1643–1661, 2016.